Journal of Alloys and Compounds 510 (2012) 1–5

Contents lists available at SciVerse ScienceDirect

Journal of Alloys and Compounds

journal homepage: www.elsevier.com/locate/jallcom

Magnetic properties of new compounds $RuMn_2Sn$ and $RuMn_2Si$

K. Endo [a], T. Kanomata [a,*], H. Nishihara [b], K.R.A. Ziebeck [c]

[a] Faculty of Engineering, Tohoku Gakuin University, Tagajo 985-8537, Japan
[b] Faculty of Science and Technology, Ryukoku University, Otsu 520-2194, Japan
[c] Department of Physics, Cavendish Laboratory, University of Cambridge, Cambridge CB3 0HE, UK

ARTICLE INFO

Article history:
Received 29 July 2011
Accepted 26 August 2011
Available online 6 September 2011

Keywords:
$RuMn_2Si$
$RuMn_2Sn$
Ferrimagnetism
Magnetic moment
Curie temperature
Spin-glass

ABSTRACT

New compounds $RuMn_2Z$ (Z = Si, Sn) have been synthesized. X-ray diffraction measurements have confirmed that $RuMn_2Z$ (Z = Si, Sn) crystallizes in a Heusler-like cubic structure. The lattice parameters of $RuMn_2Si$ and $RuMn_2Sn$ at room temperature are estimated to be 5.8260 Å and 6.2195 Å, respectively. Magnetization measurements have been carried out in fields up to 50 kOe for $RuMn_2Z$ (Z = Si, Sn). Furthermore, the temperature dependence of initial permeability of $RuMn_2Sn$ has been studied. $RuMn_2Sn$ shows ferrimagnetic behavior. The spontaneous magnetic moment at 5 K and the Curie temperature of $RuMn_2Sn$ are found to be of 1.68 μ_B/f.u. and 272.1 K, respectively. $RuMn_2Si$ exhibits spin-glass-like behavior with a freezing temperature estimated to be about 50 K.

1. Introduction

Ferromagnetic shape memory alloys (FSMAs) with the $L2_1$ structure have attracted much attention due to their potential application as smart materials [1,2]. They show a large magnetic-field-induced strain by the rearrangement of twin variants in the martensite phase [3]. Until now, several candidates for FSMAs have been reported. Among them, the stoichiometric Heusler alloy Ni_2MnGa is the most studied system. Ni_2MnGa has the cubic $L2_1$ Heusler structure at room temperature and orders ferromagnetically at a Curie temperature of 365 K. On cooling below a martensitic transition temperature of about 200 K, a superstructure forms [4]. A number of investigations on Ni–Mn–Ga FSMAs have been described in the literature because the Curie temperature and the martensitic transition temperature can be tuned by changing the composition of the constituent elements. Topics relating to Ni–Mn–Ga FSMAs have been reviewed by Entel et al. [5] and Brown et al. [6] in recent articles.

Recently, Liu et al. synthesized a new compound $NiMn_2Ga$ which carries a magnetic moment of about 1.4 μ_B/f.u. at 5 K [7]. The Curie temperature was found to be 588 K [7]. Furthermore, they reported that $NiMn_2Ga$ exhibits a martensitic transition around room temperature with a large hysteresis up to 50 K and a lattice distortion as large as 21.3%. They also observed an excellent two-way shape memory behavior with a strain of 1.7% in a single crystal. Both experimental and theoretical studies made clear that $NiMn_2Ga$ crystallizes in the Hg_2CuTi-type structure (space group $F\bar{4}3m$), which is different from the $L2_1$ structure with $Fm\bar{3}m$ space group [8]. Simultaneously, Barman et al. discussed the martensitic transition, ferrimagnetism and Fermi surface nesting using a first-principles calculation [9,10]. Liu et al. investigated theoretically and experimentally the electronic structures and magnetic properties of $CoMn_2Z$ (Z = Al, Ga, In, Si, Ge, Sn and Sb) compounds [11]. It was predicted that the compounds with Z = Al, Si, Ge, Sn and Sb are half-metallic ferrimagnets. Experimentally, they successfully synthesized the $CoMn_2Z$ (Z = Al, Ga, In, Ge, Sn and Sb) compounds and confirmed that these compounds crystallize in the Hg_2CuTi-type structure instead of the conventional $L2_1$ structure. However, there has been only a little amount of information on the magnetic moments and the exchange interactions for XMn_2Z (X = transition element: Z = s, p element) compounds. In this paper, the structural and magnetic properties of $RuMn_2Z$ (Z = Si, Sn) are examined experimentally to gain deeper insight into the magnetic moments and the exchange interactions of XMn_2Z alloys.

2. Experimental

For the preparation of the specimens, powdered ruthenium (99.9%), manganese (99.99%), silicon (99.9999%) and tin (99.99%) were mixed in the desired proportions and sealed in evacuated silica tubes. For the preparation of $RuMn_2Sn$, the mixture was first heated at 1000 °C for 3 days and then quenched into water. To achieve a high crystalline perfection, the reaction product was pulverized, carefully ground and heated again at 1050 °C for 3 days. The reaction product was then reheated to 1100 °C for 3 days and then quenched into water. For the preparation of $RuMn_2Si$, the mixture of constituents was first heated to 1100 °C for 3 days. Thereafter the reaction product was heated to 1100 °C for 3 days and then quenched into water. The

* Corresponding author. Tel.: +81 22 795 7323; fax: +81 22 368 7070.
E-mail address: kanomata@tjcc.tohoku-gakuin.ac.jp (T. Kanomata).

0925-8388/$ – see front matter © 2011 Elsevier B.V. All rights reserved.
doi:10.1016/j.jallcom.2011.08.090

observed X-ray diffraction patterns were analyzed using the Rietveld profile refinement program. The temperature dependence of the initial permeability was measured using an ac transformer method in which the primary and secondly coils were wound around a cylindrical sample of diameter ~ 1 mm and length ~ 10 mm. When an ac current of a constant amplitude flows in the primary coil, the voltage induced in the secondary coil is directly proportional to the initial permeability. Magnetization measurements on each sample were made in magnetic fields up to 50 kOe using a superconducting quantum interference device (SQUID) magnetometer.

3. Results and discussion

The Heusler $L2_1$-type structure is comprised of four interpenetrating fcc sublattices with A, B, C and D sites. The A, B, C and D sites are located at (0, 0, 0), (1/4, 1/4, 1/4), (1/2, 1/2, 1/2) and (3/4, 3/4, 3/4), respectively, as shown in Fig. 1. Fig. 2(a) shows the experimental X-ray diffraction pattern at room temperature for a powder sample of $RuMn_2Sn$. All the experimental diffraction lines can be indexed with the cubic structure. The sharp (2 2 0) peak confirms the presence of a single cubic phase. The lattice parameter a of $RuMn_2Sn$ at room temperature was found to be 6.2195 Å. The pattern in Fig. 2(b) was calculated using the $L2_1$ structure and the experimental lattice parameter, with the A and C sites occupied by the Mn atoms, and B and D sites occupied by Ru and Sn atoms, respectively. We call this structure the $L2_1$A-type. By exchanging the Mn atoms at the C sites with the Ru atoms at the B sites, the $L2_1$A-type structure changes into another ordered arrangement with a different superstructure. The prototype of this structure is the Hg_2CuTi compound which has the $F\bar{4}3m$ space group. Fig. 2(c) shows the X-ray powder diffraction pattern calculated by assuming the Hg_2CuTi-type structure. We call this structure the XA-type. The X-ray powder diffraction pattern of Fig. 2(d) was calculated by assuming that Mn atoms and Sn atoms occupy B sites and D sites, respectively, and that the other Mn atoms and Ru randomly occupy the A and C sites. This leads to the $L2_1$ structure though the atomic arrangement is different from the $L2_1$A-type structure. We call this structure the $L2_1$B-type. The intensity I of different lattice diffraction line is proportional to the square of the structure factor, $F(h\,k\,l)^2$ in which h, k and l are the Miller indices. For Heusler alloys, $F(1\,1\,1)$, $F(2\,0\,0)$ and $F(3\,1\,1)$, etc. correspond to the order-dependent superlattice diffraction lines, whilst $F(2\,2\,0)$ is an order independent fundamental diffraction line. Therefore, the different superlattice structures can be distinguished by comparing the intensity ratio

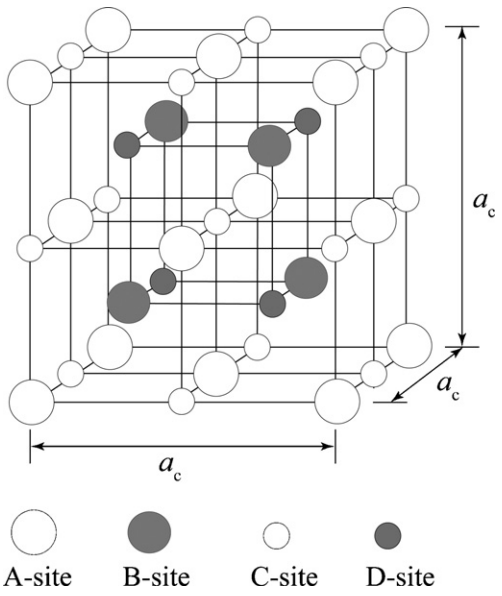

Fig. 1. Crystal structure of the Heusler-type alloy.

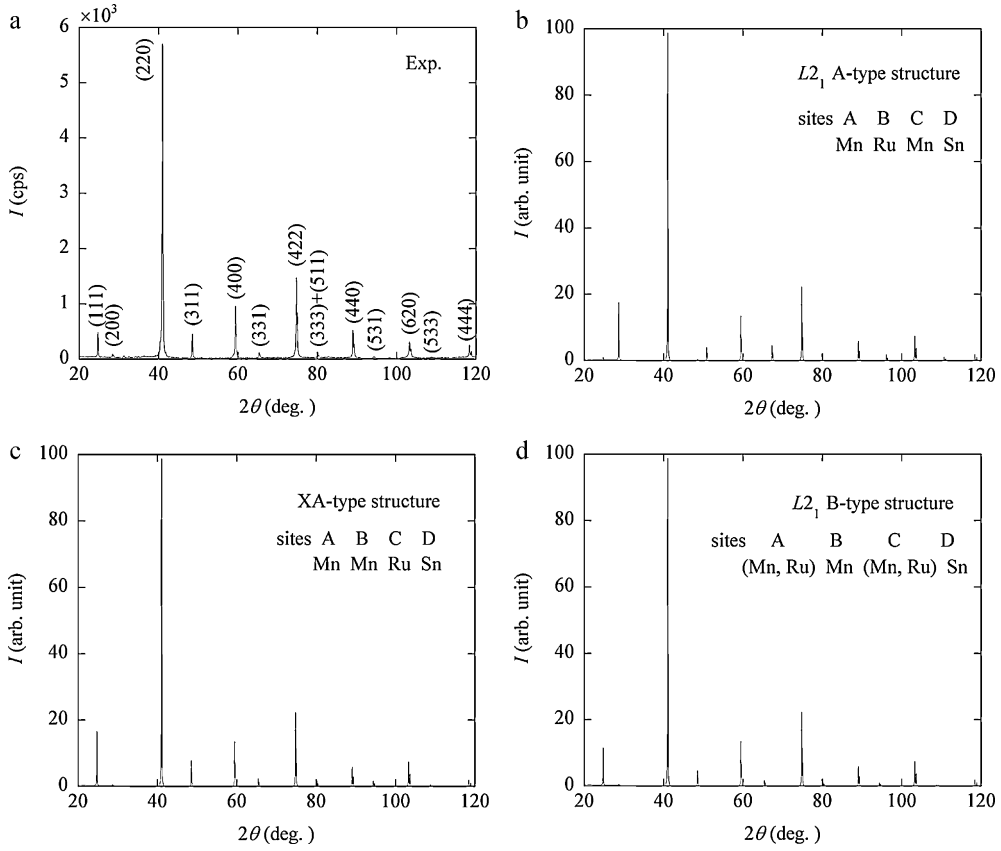

Fig. 2. Observed X-ray powder diffraction pattern at room temperature of $RuMn_2Sn$ (a). Calculated X-ray powder diffraction pattern of $RuMn_2Sn$ for the $L2_1$A-type crystal structure (b), the XA-type crystal structure (c) and the $L2_1$B-type crystal structure (d). The $L2_1$A, XA and $L2_1$B-type crystal structures are explained in the text.

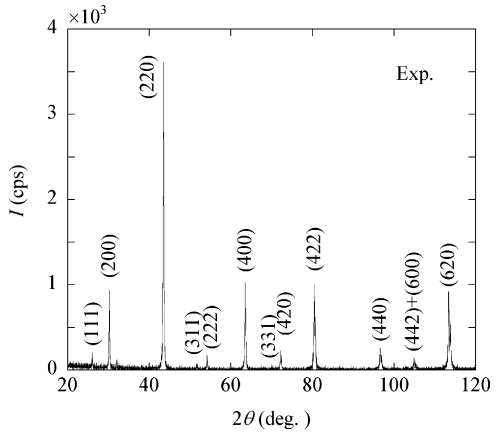

Fig. 3. Observed X-ray powder diffraction pattern at room temperature of $RuMn_2Si$.

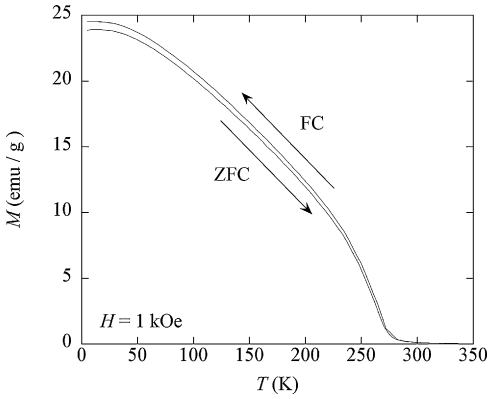

Fig. 5. Temperature dependence of the magnetization M at 1 kOe of $RuMn_2Sn$. The arrows with ZFC and FC along the curves show the zero-field-cooling and field-cooling processes, respectively.

of the different diffraction lines as $I(1\,1\,1)/I(2\,2\,0)$. The experimental results of $I(1\,1\,1)/I(2\,2\,0)$, $I(2\,0\,0)/I(2\,2\,0)$ and $I(3\,1\,1)/I(2\,2\,0)$ are in good agreement with those calculated for the $L2_1$B- or XA-type structure as shown in Fig. 2(c) and (d). It should be noted that the values of $I(1\,1\,1)/I(2\,2\,0)$ etc. are nearly comparable for the $L2_1$B- and XA-type structure. Fig. 3 shows the experimental X-ray diffraction pattern at room temperature for a powder sample of $RuMn_2Si$. Most experimental diffraction lines were indexed using the fcc cubic structure consistent with $RuMn_2Si$ also having the $L2_1$B- or XA-type structure. The lattice parameter a at room temperature of $RuMn_2Si$ was estimated to be 5.8260 Å. Liu et al. reported that $NiMn_2Ga$ crystallizes in the XA-type structure [8] but they did not consider the possibility of $L2_1$B order in their analysis of the X-ray powder diffraction pattern. Recently, Brown et al. carried out high resolution neutron diffraction measurements on $NiMn_2Ga$ [12]. They showed that the austenite phase of $NiMn_2Ga$ does not crystallize in the XA-type atomic order proposed on the basis of the X-ray measurements, but in the $L2_1$B-type crystal structure. Neutron diffraction measurements will also be necessary to establish the crystal structure of $RuMn_2Z$ (Z = Si, Sn).

The magnetization curve at 5 K for $RuMn_2Sn$ is shown in Fig. 4. The magnetization M at 5 K is saturated in a field of about 5 kOe, indicating that the magnetocrystalline anisotropy energy of $RuMn_2Sn$ is small. The spontaneous magnetization at 5 K for $RuMn_2Sn$ was determined by the linear extrapolation to $H/M = 0$ of the M^2 versus H/M curve. The magnetic moment was deduced from the value of the spontaneous magnetization at 5 K and was found to be 1.68 μ_B/f.u. It should be noted that the magnetic moment per formula unit at 5 K of $NiMn_2Ga$ has a similar value of about 1.4 μ_B [7]. The inset in Fig. 4 shows the temperature dependence of the magnetization M at 100 Oe for $RuMn_2Sn$. As shown in the figure, M decreases rapidly just below T_C and takes a nearly constant value with further rise in temperature. A linear extrapolation of these two ranges was used to obtain a point of intersection which was taken to define the Curie temperature. Using this method the Curie temperature T_C of $RuMn_2Sn$ was found to be 272.1 K. Fig. 5 shows the temperature dependence of the magnetization M in a field of $H = 1$ kOe for $RuMn_2Sn$. In a zero-field-cooled process (ZFC), a sample was first cooled to 5 K from room temperature under zero magnetic field; at this temperature the magnetic field H (=1 kOe) was applied and the magnetization was measured at this constant field with increasing temperature up to 400 K. Then, without removing the external field, the magnetization measurement was made on decreasing temperature, i.e., field-cooled (FC). The behavior of $M(T)$ for $RuMn_2Sn$ is that of a typical ferrimagnet predicted by molecular field theory on the basis of a localized model [13].

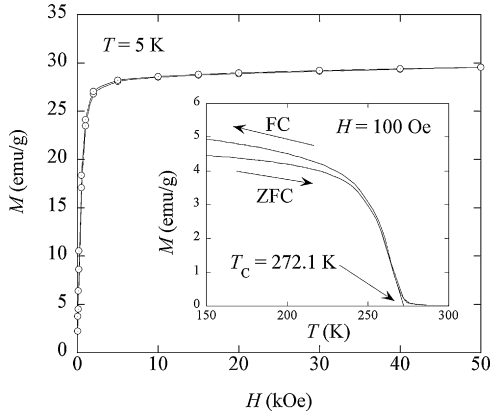

Fig. 4. Magnetization curve at 5 K of $RuMn_2Sn$. The inset shows temperature dependence of the magnetization M at 100 Oe for $RuMn_2Sn$. The arrows with ZFC and FC along the curves show the zero-field-cooling and field-cooling processes, respectively.

Ru_2MnZ (Z = Si, Ge, Sn and Sb) crystallize in the $L2_1$A-type structure [14,15]. For Ru_2MnZ (Z = Si, Ge, Sn and Sb), the Ru atoms occupy the A and C sites whilst the Mn and Z atoms occupy the B and D sites, respectively. These compounds exhibit antiferromagnetic behavior with a Néel temperature that reaches room temperature. The results of the neutron diffraction measurements for Ru_2MnZ (Z = Ge, Sn, Sb) indicate that these compounds have an antiferromagnetic type II (AF II) spin structure [16,17]. The AF II spin structure is characterized by (1 1 1) planes in which the spins are aligned ferromagnetically with adjacent planes coupled antiferromagnetically. Moreover, neutron diffraction measurements on Ru_2MnZ (Z = Ge, Sn, Sb) have shown that only the Mn atoms carry a magnetic moment with a value of about 4 μ_B. In order to examine the magnetic properties of Ru_2MnZ (Z = Si, Ge, Sn, Sb), Ishida et al. have calculated the electronic structures [18]. They established the localized nature of the Mn moment in Ru_2MnZ (Z = Si, Ge, Sn, Sb). In the case of $RuMn_2Sn$, the excess Mn atoms (MnI) occupy the A and/or C sites as shown in Fig. 1 even if $RuMn_2Sn$ crystallizes in $L2_1$B- or XA-type structure as mentioned above. We call Mn atoms on the B sublattice MnII. It is expected that the hybridization between the Ru and MnII states is stronger than that between the Ru and MnI 3d states in $RuMn_2Sn$ because the nearest neighbor distance (≈2.7 Å) between the Ru and MnII atoms is shorter than that (≈3.1 Å) between the Ru and MnI atoms. The strong hybridization pulls the MnII 3d states below the Fermi energy E_F, resulting in strong polarization and a larger moment of the MnII atoms compared to that of the MnI atoms. Recently, Barman et al. studied theoretically the electronic structure of $NiMn_2Ga$ using the full

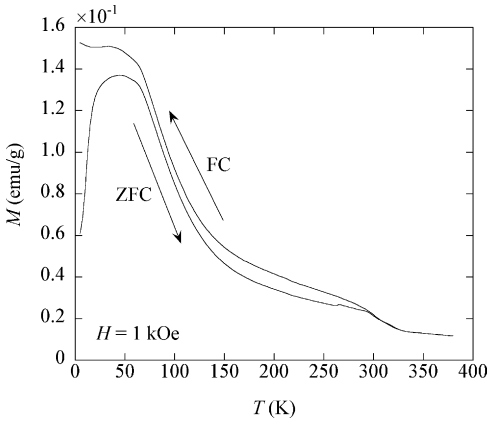

Fig. 6. Temperature dependence of the magnetization M at 1 kOe of $RuMn_2Si$. The arrows with ZFC and FC along the curves show the zero-field-cooling and field-cooling processes, respectively.

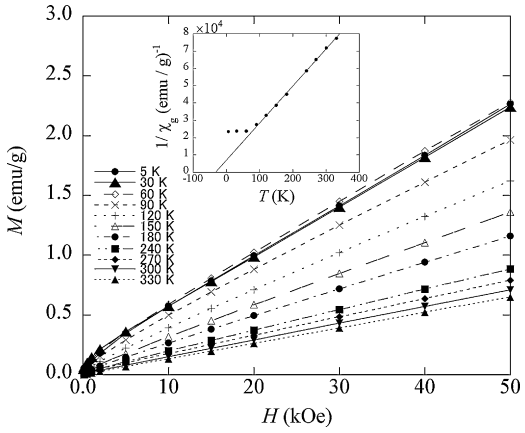

Fig. 7. Magnetization curves at various temperatures for $RuMn_2Si$. The inset shows the temperature dependence of the reciprocal susceptibility $1/\chi_g$ for $RuMn_2Si$.

potential linearized augmented plane wave method (FPLAPW) [9]. They reported that the local magnetic moment in the austenite phase of $NiMn_2Ga$ are −2.43, 3.2, 0.32 and 0.01 μ_B/f.u. for MnI, MnII, Ni and Ga, respectively. The difference between the MnI and MnII magnetic moments in $NiMn_2Ga$ may be attributed to the difference in hybridization between the Ni and MnII 3d states, and the Ni and MnI 3d states. It is well known that exchange interactions in Mn-based alloys and compounds depend strongly on the Mn–Mn distance. Yamada et al. carried out a neutron diffraction measurement of α-Mn [19]. On the basis of the localized moment model, they discussed the dependence of Mn–Mn exchange interactions on the interatomic distance. Yamada's proposition shows that the nearest neighbor Mn–Mn exchange interaction has a minimum (negative) value around the nearest neighbor Mn–Mn distance R of 2.5 Å and increases with increasing R for $R > 2.5$ Å. Kanomata et al. suggested the interaction curve for the Heusler alloys containing Mn atoms [20–22]. Recently, Şaşıoğlu et al. studied theoretically the pressure dependence of exchange interactions in the ferromagnetic Heusler alloy Ni_2MnSn [23]. Empirical and theoretical interaction curves indicate that the Mn–Mn exchange interaction at short interatomic distance becomes negative. In the present study we observed a magnetic moment of 1.68 μ_B/f.u. at 5 K for $RuMn_2Sn$. This small magnetic moment per formula unit of $RuMn_2Sn$ may be attributed to an antiferromagnetic coupling between the magnetic moments of MnI and MnII atoms, indicating that $RuMn_2Sn$ is a ferrimagnet. This is consistent with the result of the temperature dependence of the magnetization for $RuMn_2Sn$ shown in Fig. 5. Thus, the difference between MnI and MnII magnetic moments is a key to the magnetic moment per formula unit of 1.68 μ_B for $RuMn_2Sn$.

Fig. 6 shows the temperature dependence of the magnetization in 1 kOe of $RuMn_2Si$ for ZFC and FC processes. As shown in the figure, the magnetization for the ZFC process makes a broad maximum at about 50 K. With decreasing temperature, the magnetization decreases steeply. On the other hand, in the case of the FC process, the magnetization is almost constant below about 50 K. This behavior is typical for a spin-glass-like magnet with a freezing temperature T_f of about 50 K. Above T_f the magnetization decreases with increasing temperature but exhibits an anomaly around 300 K. Fig. 7 shows the magnetization curves of $RuMn_2Si$ for $5 \le T \le 330$ K and in magnetic fields up to 50 kOe. As seen in the figure, the magnetization increases linearly with increasing applied field. From 5 K to 270 K a small ferromagnetic component can be observed in the magnetization curves. Thus, the anomaly at about 300 K in the M versus T curves of Fig. 6 is due to the contribution of a small amount of ferromagnetic impurity in $RuMn_2Si$. We determined the temperature dependence of the magnetic susceptibility χ_g for $RuMn_2Si$ from the slope of the magnetization curves in Fig. 7. The observed $1/\chi_g$ versus T curve is shown in the inset in Fig. 7. Above about 100 K the curve follows a Curie–Weiss law. From this result, the paramagnetic Curie temperature θ_p and the effective paramagnetic moment p_{eff} were determined to be −36 K and 3.0 μ_B/f.u., respectively. In the case of $RuMn_2Si$, the value of the paramagnetic Curie temperature is negative, indicating that the antiferromagnetic interaction is a predominant exchange interaction. It is not clear why $RuMn_2Si$ exhibits spin-glass-like behavior.

4. Summary

New compounds $RuMn_2Si$ and $RuMn_2Sn$ were synthesized in this study. X-ray measurements on $RuMn_2Si$ and $RuMn_2Sn$ have confirmed that these compounds have the Heusler-like cubic structure. The lattice constants of $RuMn_2Si$ and $RuMn_2Sn$ at room temperature are 5.8260 Å and 6.2195 Å, respectively. $RuMn_2Sn$ shows the ferrimagnetic behavior. The Curie temperature and the magnetic moment per formula unit at 5 K of $RuMn_2Sn$ are found to be 272.1 K and 1.68 μ_B, respectively. $RuMn_2Si$ exhibits the spin-glass-like behavior. The freezing temperature is found to be about 50 K.

Acknowledgements

The authors would like to express sincere thanks to Professor S. Fujii at Kagoshima University for his helpful discussions. This work was partly supported by a grant based on the High-Tech Research Center Program for private universities from the Japan Ministry of Education, Culture, Sports, Science and Technology. This work was also supported by a Grant-in-Aid for Scientific Research (C) (Grant No. 21560693), provided by the Japan Society for the Promotion of Science.

References

[1] A. Planes, L. Mañosa, A. Saxena (Eds.), Magnetism and Structure in Functional Materials, Springer-Verlag, Berlin, 2005.
[2] V.A. Chernenko (Ed.), Advances in Shape Memory Materials, Trans. Tech. Publications, Switzerland, 2009.
[3] K. Ullakko, J.K. Huang, C. Kantner, R.C. O'Handley, V.V. Kokorin, Appl. Phys. Lett. 69 (1996) 1966.
[4] P.J. Brown, J. Crangle, T. Kanomata, M. Matsumoto, K.-U. Neumann, B. Ouladdiaf, K.R.A. Ziebeck, J. Phys.: Condens. Matter 14 (2002) 10159.
[5] P. Entel, V.D. Buchelnikov, V.V. Khovailo, A.T. Zayak, W.A. Adeagbo, M.E. Gruner, H.C. Herper, E.E. Wassermann, J. Phys. D: Appl. Phys. 39 (2006) 865.
[6] P.J. Brown, A.P. Gandy, K. Ishida, R. Kainuma, T. Kanomata, M. Matsumoto, H. Morito, K.-U. Neumann, K. Oikawa, B. Ouladdiaf, K.R.A. Ziebeck, J. Magn. Magn. Mater. 310 (2007) 2755.

[7] G.D. Liu, J.L. Chen, Z.H. Liu, X.F. Dai, G.H. Wu, B. Zhang, X.X. Zhang, Appl. Phys. Lett. 87 (2005) 262504.
[8] G.D. Liu, X.F. Dai, S.Y. Yu, Z.Y. Zhu, J.L. Chen, G.H. Wu, H. Zhu, J.Q. Xiao, Phys. Rev. B 74 (2006) 054435.
[9] S.R. Barman, S. Banik, A.K. Shukla, C. Kamal, A. Chakrabarti, Europhys. Lett. 80 (2007) 57002.
[10] S.R. Barman, A. Chakrabarti, Phys. Rev. B 77 (2008) 176401.
[11] G.D. Liu, X.F. Dai, H.Y. Liu, J.L. Chen, Y.X. Li, G. Xiao, G.H. Wu, Phys. Rev. B 77 (2008) 014424.
[12] P.J. Brown, T. Kanomata, K. Neumann, K.-U. Neumann, B. Ouladdiaf, A. Sheikh, K.R.A. Ziebeck, J. Phys.: Condens. Matter 22 (2010) 506001.
[13] L. Néel, Ann. Phys. (Paris) 3 (1948) 137.
[14] T. Kanomata, M. Kikuchi, H. Yamauchi, T. Kaneko, Jpn. J. Appl. Phys. 32 (Suppl. 3) (1993) 292.
[15] T. Kanomata, M. Kikuchi, H. Yamauchi, J. Alloys Compd. 414 (2006) 1.
[16] M. Gotoh, M. Ohashi, T. Kanomata, Y. Yamaguchi, Physica B 213–214 (1995) 306.
[17] M. Gotoh, MS Thesis, Tohoku University, 1995.
[18] S. Ishida, S. Kashiwagi, S. Fujii, S. Asano, Physica B 210 (1995) 140.
[19] T. Yamada, N. Kunitomi, Y. Nakai, D.E. Cox, G. Shirane, J. Phys. Soc. Jpn. 28 (1970) 615.
[20] T. Kanomata, K. Shirakawa, T. Kaneko, J. Magn. Magn. Mater. 65 (1987) 76.
[21] K. Shirakawa, T. Kanomata, T. Kaneko, J. Magn. Magn. Mater. 70 (1987) 421.
[22] Y. Chieda, T. Kanomata, K. Fukushima, K. Matsubayashi, Y. Uwatoko, R. Kainuma, K. Oikawa, K. Ishida, K. Obara, T. Shishido, J. Alloys Compd. 486 (2009) 51.
[23] E. Şaşıoğlu, L.M. Sandratskii, P. Bruno, Phys. Rev. B 71 (2005) 214412.